

QUANTIFYING LAND AERIAL RESCUE DEMAND INTENSITY: A DATA-DRIVEN MODELING APPROACH FOR DEFINING THE AIR-GROUND OPERATIONAL BOUNDARY

WANG Gaofeng[1], CHENG Wenyuan[1], WU Yangmeng[1] & ZHAO Luodi[1]

[1]Aeronautical Science and Technology Strategy and Systems Engineering Research Division, Aviation Industry Development Research Center of China (ADR), Beijing 100029, China

Abstract

This paper proposes the Aerial Rescue Demand Intensity (ARDI) index and a spatial assessment method to address two persistent challenges in large-scale land search and rescue (SAR): the lack of a quantitative aerial-rescue demand surface and the absence of a unified demand-side criterion for distinguishing the relative roles of aerial and ground response. ARDI decomposes aerial-rescue demand into Land Rescue Demand Intensity (LDI) and the Aerial Relative Necessity Index (ANI). LDI uses ambient population as a proxy for the size of the potentially exposed population and incorporates terrain-induced, weather-related, and thermal-physiological hazards. ANI characterizes the extent to which ground-access conditions allow ground response to substitute for aerial response, based on road-support deficiency and terrain constraints. Their multiplicative coupling identifies areas that combine meaningful rescue demand with a high relative necessity for aerial intervention. Using multisource geospatial data, the framework is applied to China on a common $0.1^\circ \times 0.1^\circ$ grid. LDI is generally higher in eastern and southern China, whereas ANI is higher across western plateaus and border regions. ARDI hotspots concentrate where human activity overlaps with complex mountain, plateau, and border-transition environments. The resulting spatial pattern can be descriptively summarized as four principal regions, four secondary belts, and one island. Thresholds derived from representative critical scenarios classify valid land cells into low-demand, ground-dominant, aviation-assisted, aviation-dependent, and high-aviation-demand zones, accounting for 37.62%, 32.06%, 19.23%, 5.92%, and 5.16%, respectively. The three zones with clear value for aerial intervention account for 30.31%, while aviation-dependent and high-aviation-demand zones together account for 11.08%. The method integrates demand identification, aerial-necessity assessment, and demand-side air-ground functional zoning, providing a quantitative basemap for the spatial analysis and regional prioritization of aerial-rescue demand.

Keywords: Aerial Rescue; Land Search and Rescue; Aerial Rescue Demand Intensity; Air-Ground Operational Boundary; Geospatial Analysis

1. Introduction

Land search and rescue (SAR) is characterized by sudden onset, uncertain incident locations, narrow response windows, and pronounced variation in operating environments. Incidents may occur along densely populated urban fringes and transport corridors, as well as in mountains, plateaus, forests, deserts, and border regions. Spatial differences in human activity, environmental hazards, and responder accessibility therefore produce a highly heterogeneous distribution of land-SAR demand. A fundamental question in land-rescue-system planning is therefore where rescue demand is relatively high.

Within land SAR, aerial and ground response have different spatial operating characteristics. Aerial rescue can bypass complex terrain and surface-transport barriers, rapidly reach an incident area,

https://doi.org/10.71945/icas2026_0298

and support wide-area search, rescue-team insertion, medical evacuation, and cross-regional support. Ground response relies more strongly on surface accessibility and continuous approach routes. Aerial-rescue demand therefore depends on both the presence of meaningful rescue demand and the relative importance of aerial response under local access conditions. A densely populated area with a well-developed road network may generate substantial land-rescue demand with low relative aerial necessity, while an environmentally extreme but virtually uninhabited area may generate limited aerial-rescue demand.

At the planning level, spatial demand assessment establishes a demand-side basemap of where rescue demand is concentrated and where aerial response becomes comparatively important relative to ground response. The present study constructs this spatial representation at the grid-cell level. ARDI expresses the intrinsic distribution of aerial-rescue demand generated by population exposure, environmental hazards, and ground-access conditions.

A demand-side assessment therefore addresses two related questions: whether meaningful rescue demand exists, and whether aerial intervention becomes comparatively necessary when that demand arises.

Existing SAR-planning research has largely followed two methodological streams. The first uses isochrones or reachable-area analysis, taking base locations, aircraft performance, and mission-time constraints as inputs to estimate the area that can be reached within a prescribed time and thereby evaluate the coverage of helicopters or other aerial assets [1]. The second applies location-allocation optimization, formulating base siting and resource assignment as facility-location problems that maximize coverage, minimize response time, or optimize an integrated effectiveness measure [2]. These approaches address resource configuration after a demand surface has been specified. Their treatment of demand as an externally supplied input leaves the spatial formation of demand from population activity, environmental hazards, and ground accessibility insufficiently characterized. Some studies have introduced traffic flow, historical accident frequency, and related variables to construct rescue-demand indicators for specific scenarios [3]. Such methods generally depend on regional incident records and have limited transferability to large land areas where historical data are sparse or compiled under inconsistent statistical definitions. A generic rescue hotspot also provides only part of the information required to characterize the relative role of aerial response. A demand-side framework that jointly quantifies land-rescue demand, the relative necessity of aerial intervention, and their spatial boundary remains lacking.

To construct this demand-side basemap, this study proposes the Aerial Rescue Demand Intensity (ARDI) index as a spatial demand-assessment method for large-scale land SAR. The framework separates aerial-rescue demand into two connected but functionally distinct components. Land Rescue Demand Intensity (LDI) represents the relative level of potential personnel-rescue demand in a spatial unit; it uses ambient population as a proxy for the size of the potentially exposed population and incorporates terrain-induced, weather-related, and thermal-physiological hazards. The Aerial Relative Necessity Index (ANI) represents the relative necessity of aerial response when a rescue need arises; it characterizes the extent to which ground-access conditions allow ground response to substitute for aerial response, based on road-support deficiency and terrain constraints. The LDI-ANI indicator space delineates the demand-side air-ground operational boundary and classifies the continuous demand surface into low-demand, ground-dominant, aviation-assisted, aviation-dependent, and high-aviation-demand zones. The resulting demand basemap supports spatial interpretation and regional prioritization of aerial-rescue demand.

2. Conceptual Framework and Overall ARDI Model

2.1 ARDI Construction

A regular spatial grid is adopted as the basic analytical unit, with an arbitrary cell denoted by s. A cell constitutes an area of high aerial-rescue demand only when it combines substantial land-rescue demand with a high relative necessity for aerial intervention. Where demand exists and ground accessibility remains strong, aerial response serves a complementary role. Where demand exists and ground access is severely constrained, the relative necessity of aerial response becomes high. The ARDI framework is organized into four analytical layers.

At the first layer, the reported Aerial Rescue Demand Intensity, $ARDI(s)$, is an order-preserving transformation of the underlying aerial-rescue demand score for land SAR, $Q_A(s)$:

$$ARDI(s) = g[Q_A(s)] \tag{1}$$

Here, $g(\cdot)$ is a monotonically increasing function used for scale compression, index presentation, or normalization. It improves comparability without changing the spatial ranking. Where $Q_A(s)$ is already interpretable, the identity transformation $g[Q_A(s)] = Q_A(s)$ may be used.
At the second layer, the underlying aerial-rescue demand score for land SAR is obtained by coupling LDI with ANI:

$$Q_A(s) = LDI(s)ANI(s) \tag{2}$$

$LDI(s)$ describes whether potential land-rescue demand exists and how strong it is, whereas $ANI(s)$ describes whether aerial response is comparatively more necessary than ground response when such demand occurs. The multiplicative structure prevents cells without an exposed population from being classified as having high aerial-rescue demand and also prevents highly populated or hazardous areas in which ground response can readily substitute for aerial response from being classified as aviation-dependent solely on the basis of demand magnitude.
At the third layer, ANI is determined jointly by road-access support and terrain constraints on ground rescue:

$$ANI(s) = \Psi[RA(s), TG(s)] \tag{3}$$

Here, $RA(s)$ denotes road-access support, $TG(s)$ denotes the degree to which terrain constrains ground rescue, and $\Psi(\cdot)$ is the ANI aggregation function. Better road support increases ground accessibility and reduces the relative necessity of aviation, whereas stronger terrain constraints reduce ground-mobility efficiency and increase aerial necessity.
At the fourth layer, LDI is constructed from an exposure basis and environmental hazards:

$$LDI(s) = \Phi[B(s), H(s)] \tag{4}$$

where $B(s)$ is the demand basis, $H(s)$ is the environmental-hazard index, and $\Phi(\cdot)$ is the aggregation function. In the proxy model developed here, this relationship is instantiated as:

$$LDI(s) = \Phi[P_a(s), H_{te}(s), H_{we}(s), H_{th}(s)] \tag{5}$$

$P_a(s)$ is ambient-population exposure and serves as the proxy for $B(s)$. The terms $H_{te}(s)$, $H_{we}(s)$, and $H_{th}(s)$ represent terrain-induced, weather-induced, and thermal-physiological hazards, respectively. The function $\Phi(\cdot)$ describes how exposed population and environmental hazards combine to generate relative land-rescue demand.
This four-layer structure separates the questions of demand existence and aerial necessity. LDI measures the intensity of potential rescue demand, ANI measures the relative need for aviation, and ARDI identifies locations where both conditions jointly create planning-relevant aerial-rescue demand.

2.2 Indicator Normalization

The underlying indicators differ substantially in units, ranges, and distributional shape. Before aggregation, they are transformed using semi-saturation functions. For indicators positively associated with demand, hazard, or aerial necessity, the forward function is:

$$F^{+}(x, x_0, \alpha) = \left(\frac{x}{x + x_0}\right)^{\alpha} \tag{6}$$

For indicators negatively associated with demand, hazard, or aerial necessity, the inverse function is:

$$F^{-}(x, x_0, \alpha) = \left(\frac{x_0}{x + x_0}\right)^{\alpha} \tag{7}$$

In these expressions, x is the raw indicator, x_0 is the scale parameter, and α is the shape parameter. When $\alpha = 1$, x_0 is a strict half-saturation scale and the normalized response equals 0.5 at $x = x_0$. When $\alpha \neq 1$, x_0 remains the characteristic transition scale, while α controls the steepness of the response. The forward function is used for ambient population, terrain complexity, weather hazards, and thermal stress; the inverse function is used for road-access support.

Semi-saturation normalization is adopted for three reasons. First, it maps heterogeneous indicators into a comparable dimensionless space. Second, it captures diminishing marginal effects. For example, adding a small amount of road access in a roadless area can substantially improve ground-rescue accessibility, whereas an equivalent increase within a dense urban network has a much smaller effect on the air-ground substitution relationship. Third, the scale parameter x_0 can shift the model's discrimination toward lower or higher indicator ranges according to the planning objective.

2.3 Shifted Multiplicative Aggregation Model

The assessment combines ambient population, environmental hazards, road support, and topographic constraints. These factors can reinforce one another, requiring an aggregation operator that represents compound effects rather than simple addition. Drawing on the structural logic of multiplicative multiattribute utility functions [4] and geometric aggregation in composite-indicator construction [5, 6], this study introduces a Shifted Multiplicative Aggregation Model (SMAM).

For n directionally harmonized and dimensionless indicators $x_i(s) \geq 0$, SMAM is defined as:

$$I(s) = \prod_{i=1}^{n} [1 + \lambda_i x_i(s)]^{\kappa w_i} - 1 \tag{8}$$

subject to:

$$w_i \geq 0, \qquad \sum_{i=1}^{n} w_i = 1, \qquad \lambda_i > 0, \qquad \kappa > 0 \tag{9}$$

where w_i is the relative weight, λ_i is an indicator-response coefficient, and κ is the aggregation-intensity parameter. The constant 1 provides the shift that prevents the entire aggregate from collapsing to zero when one indicator is zero. Structurally, $1 + \lambda_i x_i(s)$ can be interpreted as the impact multiplier of factor i relative to a no-adverse-condition baseline; multiplication represents the compound amplification produced when several adverse factors coexist.

When $\kappa = 1$ and $\lambda_i = 1$, SMAM reduces to a shifted weighted geometric mean:

$$I(s) = \prod_{i=1}^{n} [1 + x_i(s)]^{w_i} - 1 \tag{10}$$

If all inputs are equal, the aggregate equals the common input. This form is therefore suitable for combining multiple proxy indicators within a single conceptual dimension and prevents a dimension from receiving additional structural weight merely because it contains more sub-indicators.

When $\kappa = n$, $w_i = 1/n$, and $\lambda_i = 1$, SMAM reduces to:

$$I(s) = \prod_{i=1}^{n} [1 + x_i(s)] - 1 \tag{11}$$

This form is suitable for compound enhancement among relatively independent hazard or rescue-difficulty dimensions. If only one indicator is nonzero, the aggregate reduces to that indicator, preserving scale consistency. When several dimensions increase simultaneously, the interaction terms produce a stronger response than simple addition.

2.4 Air-Ground Operational Boundary Definition

The air-ground operational boundary describes the demand-side transition from ground-dominant response to a high relative necessity for aerial response. It is a demand-side functional boundary jointly determined by LDI and ANI. The boundary is first defined in the two-dimensional LDI-ANI space and then projected onto geographic space to establish demand-side air-ground functional zoning for each cell.

Let $L(s) = LDI(s)$, $N(s) = ANI(s)$, and $A(s) = ARDI(s)$. Given land-rescue-demand thresholds τ_{L0} and τ_{L1}, an aerial-necessity threshold τ_N, and a significant aerial-demand threshold τ_A, cells are divided into five classes.

The threshold τ_A identifies whether a cell enters a planning-relevant aerial-demand range. The thresholds τ_{L0} and τ_{L1} represent minimum effective and high land-rescue demand, respectively, while τ_N identifies the transition from ground accessibility to a high relative necessity for aerial response. Thresholds can be established either statistically, using quantiles for large-area comparison, or physically, by inverting the model for a representative critical scenario such as a cell with sustained ambient-population exposure, insufficient road support, and strong terrain constraints.

Table 1 – Decision rules for the demand-side air-ground operational boundary.

Zone	Mathematical criterion	Demand-side interpretation
Low demand	$L(s) < \tau_{L0}$	Potential rescue demand remains below the minimum effective-demand threshold.
Ground-dominant	$L(s) \geq \tau_{L0}, N(s) < \tau_N, A(s) < \tau_A$	Demand is non-negligible, while road and terrain conditions support ground-led response.
Aviation-assisted	$L(s) \geq \tau_{L0}, N(s) < \tau_N, A(s) \geq \tau_A$	Ground-access conditions remain comparatively favorable, while the demand level gives aerial intervention clear relative value.
Aviation-dependent	$\tau_{L0} \leq L(s) < \tau_{L1}, N(s) \geq \tau_N$	Demand is low to moderate, while ground-access constraints produce a high relative necessity for aerial response.
High-aviation-demand	$L(s) \geq \tau_{L1}, N(s) \geq \tau_N$	Both rescue demand and aerial necessity are high; these cells form the highest-priority areas on the aerial-rescue demand basemap.

3. Data Sources and Spatial Pre-processing

The data cover four principal categories: population exposure, road support, terrain conditions, and weather-related hazards. LandScan Global 2024 [10] represents the baseline size of the potentially exposed population, while a 2024 OpenStreetMap (OSM) road extract is screened by road class and aggregated to the analysis grid to form the road-density indicator. Terrain data include the Relief Degree of Land Surface (RDLS) and terrain roughness, which describe both geographic mobility constraints and terrain-induced risk. The meteorological hazard layers are constructed from 2025 records: monthly mean 10-m wind fields from the ERA5 monthly averaged single-level product, daily precipitation flux and FAO-56 reference evapotranspiration from AgERA5 v2.0.0, and monthly UTCI statistics from ERA5-HEAT v1.1 [12, 13, 14]. These variables characterize strong-wind, dryness, heavy-rainfall, and extreme heat and cold hazards.

Table 2 – Data sources and spatial resolutions.

Dataset	Source	Native resolution	Target resolution	Application
LandScan Global 2024	ORNL	30 arc-seconds (approximately 1 km)	$0.1° \times 0.1°$	Ambient-population exposure
Road density (2024)	OSM	Vector data	$0.1° \times 0.1°$	Ground-access support
RDLS	GeoDOI	1 km $\times$ 1 km	$0.1° \times 0.1°$	Geographic mobility constraint
Terrain roughness	NASADEM; GeoDOI	1 arc-second $\times$ 1 arc-second; 1 km $\times$ 1 km	$0.1° \times 0.1°$	Terrain-induced hazard
Wind (2025)	ERA5 monthly means	$0.25° \times 0.25°$	$0.1° \times 0.1°$	Strong-wind hazard

Table 2 – Data sources and spatial resolutions.

Dataset	Source	Native resolution	Target resolution	Application
Dryness-heavy-rain risk (2025)	AgERA5 v2.0.0; FAO-56	$0.1° \times 0.1°$	$0.1° \times 0.1°$	Dryness and heavy-rain hazards
UTCI risk (2025)	ERA5-HEAT v1.1	$0.25° \times 0.25°$	$0.1° \times 0.1°$	Thermal-physiological hazard

All layers are harmonized to a common $0.1° \times 0.1°$ grid and a consistent land mask. Data with finer native resolution are aggregated within each target cell: population is summed, retained road length is accumulated and divided by cell area, and terrain rasters are spatially averaged. Coarser ERA5 wind and UTCI variables are resampled using spatial interpolation. This harmonization ensures that all factors share the same geographic extent, grid geometry, and masking boundary before index construction.

4. Aerial Relative Necessity and Air-Ground Boundary Model

The Aerial Relative Necessity Index, $ANI(s)$, describes the relative necessity of aerial intervention when a rescue need arises in cell s. ANI is constructed from two dimensions. Insufficient road support indicates the absence of continuous constructed access corridors. Strong terrain constraints indicate that, even where local roads or off-road routes exist, ground mobility may remain restricted by elevation, relief, and surface fragmentation. These dimensions are partially independent but can reinforce one another when they coexist.

Using the SMAM formulation in Section 2.3, ANI is defined as:

$$\begin{aligned} ANI(s) &= \left[1+\widehat{C}_r(s)\right]\left[1+\widehat{C}_t(s)\right]-1 \\ &= \widehat{C}_r(s)+\widehat{C}_t(s)+\widehat{C}_r(s)\widehat{C}_t(s) \end{aligned} \tag{12}$$

The normalized terms $\widehat{C}_r(s)$ and $\widehat{C}_t(s)$ represent road-support deficiency and terrain constraints on ground rescue, respectively. The first two terms of the expanded expression are their independent contributions, and the product term represents structural amplification when both constraints coexist. If either component is zero, ANI reduces to the other component and remains scale-consistent. If both increase, ANI grows faster than a simple sum, representing the accelerated reduction in the extent to which ground response can substitute for aerial response under the combined effects of sparse roads and difficult terrain. Because both normalized components lie in $[0,1]$, the theoretical range of ANI is $[0,3]$. A larger ANI indicates stronger overall constraints on ground response and a greater relative need for aerial rescue.

4.1 Retained Road Network and Road Support Index

Road networks are the primary infrastructure through which ground teams reach an incident area and conduct search, access, and casualty transport. Higher road density generally provides more usable approach routes per unit area, better continuity of ground coverage, and greater route-choice flexibility. Sparse roads create large uncovered areas, force detours, or require off-road movement, thereby increasing ground-rescue difficulty and the relative value of aviation.

A retained road network is constructed from a 2024 OSM vector extract. OSM provides openly contributed road features whose classes are represented by attributes such as `highway=*` [7]. Land rescue may use not only high-capacity motor roads but also rural tracks, forest roads, internal service roads, and foot-access paths for final approach. The road categories retained in this study are listed in Table 3.

Table 3 – OSM road categories retained in the model.

Functional category	OSM road class	Description
Motorways and express roads	motorway, motorway_link, trunk, trunk_link	Motorways, expressways, rapid bridge/tunnel links, interchanges, and ramps
Urban arterial roads	primary, primary_link, secondary, secondary_link	Primary and secondary urban vehicle roads and their connectors
Urban collector roads	tertiary, tertiary_link	Urban collectors, airport access roads, and connectors
Residential streets	residential	Vehicle-access streets within residential areas
Rural and suburban tracks	track, tracktype=grade1-grade5	Rural, agricultural, industrial, mining, and forest tracks
Internal and service access	living_street, path, service	Internal or access roads in residential areas, parks, stations, terminals, parking facilities, and public buildings

After the retained vector roads are clipped to the analysis grid, road density is calculated as:

$$RD(s) = \frac{\sum_{e \in E} \text{length}(e \cap s)}{A(s)} \tag{13}$$

where E is the screened set of retained road features, $e \cap s$ is the portion of road feature e within cell s, and $A(s)$ is the actual land-surface area of the cell. Road density, rather than total road length, removes the area distortion associated with latitude-dependent geographic grid cells.
Because road density is negatively associated with aerial necessity, it is transformed into a road-support-deficiency index using the inverse semi-saturation function:

$$\widehat{C}_r(s) = \frac{RD_{25\%nzp}}{RD(s) + RD_{25\%nzp}} \tag{14}$$

Here, $RD_{25\%nzp}$ is the 25th percentile among nonzero road-density cells. Excluding roadless cells from the scale estimate prevents zeros from directly determining the normalization constant. The lower quartile of road-covered areas represents the characteristic transition from very weak to ordinary road support and compresses the extreme values of dense urban and transport-hub networks. When $RD(s) = 0$, $\widehat{C}_r(s) = 1$, indicating severe road-support deficiency. The index approaches zero as road density increases and the capacity of ground response to substitute for aerial response increases.

4.2 Topographic Constraint for Ground Rescue

Terrain also directly affects ground-rescue mobility. High elevation and large-scale surface relief can increase detour distance, reduce travel speed, restrict feasible directions of movement, and limit final-area search. This study uses RDLS to represent the integrated topographic constraint on ground rescue.
RDLS combines mean elevation with local surface incision and is a widely used descriptor of regional macro-topography [8]. The 1-km Chinese RDLS dataset published through GeoDOI [9] is based on digital elevation data and is expressed as:

$$RDLS(s) = \frac{ALT(s)}{1000} + \frac{(H_{\max} - H_{\min})\,[1 - P(A,s)/A]}{500} \tag{15}$$

where $ALT(s)$ is mean elevation in the analysis window, H_{max} and H_{min} are the maximum and minimum elevations, A is the total window area, and $P(A,s)$ is the area of flat surface. The first term represents the overall elevation level. The second represents local relief and surface incision: $H_{max} - H_{min}$ is the maximum relative elevation difference, while $1 - P(A,s)/A$ is the proportion of non-flat terrain and reduces the influence of isolated elevation extremes. The denominator of 500 m provides the reference mountain-height scale used in the RDLS formulation.

After the original RDLS data are aggregated to the target grid, the terrain-constraint index is calculated using a forward semi-saturation function:

$$\widehat{C}_t(s) = \frac{RDLS(s)}{RDLS(s) + RDLS_{75\%p}} \tag{16}$$

where $RDLS_{75\%p}$ is the nationwide 75th percentile. This scale emphasizes discrimination among topographically difficult areas while reducing the dominance of extensive plains.

5. Land Rescue Demand Intensity Proxy Model

Land Rescue Demand Intensity, $LDI(s)$, represents the relative level of potential personnel-rescue demand in cell s. It is decomposed into a demand basis $B(s)$ and an environmental-hazard index $H(s)$, coupled multiplicatively as:

$$LDI(s) = \Phi[B(s), H(s)] = \widehat{P}_a(s)\, H(s) \tag{17}$$

The normalized ambient-population exposure $\widehat{P}_a(s)$ is the proxy for $B(s)$, while $H(s)$ describes how natural conditions amplify both incident likelihood and consequence severity. Potential rescue demand arises from the joint presence of exposed people and hazardous conditions. Ambient population determines the scale of people who may be affected; the hazard index determines the relative demand associated with each unit of exposure. If ambient population is zero, severe environmental conditions alone do not create personnel-rescue demand within the scope of this model. Likewise, if the modeled hazards are negligible, no additional hazard-driven demand is produced.
Using SMAM, the general environmental-hazard index is:

$$H(s) = \prod_{i=1}^{n} [1 + x_i(s)] - 1 \tag{18}$$

where $x_i(s)$ is the directionally harmonized and normalized value of hazard dimension i. The current proxy model includes terrain-induced risk, weather-induced risk, and thermal-physiological risk, denoted by $\widehat{H}_{te}(s)$, $\widehat{H}_{we}(s)$, and $\widehat{H}_{th}(s)$, respectively:

$$H(s) = \left[1 + \widehat{H}_{te}(s)\right] \left[1 + \widehat{H}_{we}(s)\right] \left[1 + \widehat{H}_{th}(s)\right] - 1 \tag{19}$$

The subtraction of 1 preserves the zero baseline and maintains consistency with the general SMAM definition. Additional hazard dimensions may be introduced as new multiplicative terms, provided they are normalized in the same direction and do not duplicate mechanisms already represented by existing variables.

5.1 Population Exposure Basis

LandScan Global 2024 ambient-population data are used to represent the demand basis [10]. The LandScan framework combines census information with roads, terrain, land cover, and other geospatial covariates to allocate population to regular grid cells and estimate typical 24-h population distribution and exposure [11]. Compared with statistics tied to registered residential locations, ambient population better represents the number of people actually likely to be present within a cell and exposed to environmental hazards.
The native LandScan raster is summed to the $0.1° \times 0.1°$ analysis grid to obtain $P_a(s)$ and is then normalized as:

$$\widehat{P}_a(s) = \frac{P_a(s)}{P_a(s) + P_{a,25\%nzp}} \tag{20}$$

where $P_{a,25\%nzp}$ is the 25th percentile among cells with nonzero ambient population. This choice shifts the half-response point toward sparsely populated areas and compresses extreme population concentrations, limiting the dominance of metropolitan cells in a nationwide assessment.

5.2 Terrain-Induced Risk

Complex terrain can increase the likelihood of falls, disorientation, entrapment, and excessive physical exertion and can prolong exposure to adverse outdoor conditions. Unlike Section 4.2, which uses the full RDLS index to describe the combined mobility constraint on rescuers, this section extracts the relative-relief component to characterize how local terrain fragmentation increases risk to exposed persons:

$$\begin{cases} Ro(s) = \dfrac{(H_{\max} - H_{\min})\,[1 - P(A,s)/A]}{500}, \\ \widehat{H}_{te}(s) = \dfrac{Ro(s)}{Ro(s) + Ro_{75\%p}} \end{cases} \tag{21}$$

The 75th percentile of relative relief is used as the transition scale from ordinary to significant terrain-induced risk. Larger $Ro(s)$ and $\widehat{H}_{te}(s)$ indicate stronger alternation of slopes and valleys, greater surface incision, and more rapid changes in terrain orientation, which tend to increase the risk of falls, disorientation, entrapment, and fatigue.

5.3 Weather-Induced Risk

Weather affects outdoor safety, environmental stability, and the severity of incident consequences. In addition to thermal-physiological stress, the model includes strong-wind risk and a combined dryness-heavy-rain risk. The first describes the persistent background hazard associated with strong winds; the second captures both long-duration water-deficit conditions and short-duration heavy-rain events. The weather-hazard index is constructed as a shifted geometric mean:

$$\widehat{H}_{we}(s) = \left\{ \left[1 + \widehat{h}_{wind}(s)\right] \left[1 + \widehat{h}_{DH}(s)\right] \right\}^{1/2} - 1 \tag{22}$$

where $\widehat{h}_{wind}(s)$ and $\widehat{h}_{DH}(s)$ are normalized wind and dryness-heavy-rain hazards. The form is idempotent: if both inputs are equal, the aggregate equals that common value, and the output remains in $[0,1]$.

5.3.1 Wind-Induced Risk

Strong winds increase the likelihood of instability, falls, and route deviation in open terrain, mountains, and elevated locations. Blowing dust, drifting snow, and the movement of trees or loose objects can further reduce visibility and operational safety. Monthly mean 10-m wind speed for 2025 is obtained from the ERA5 monthly averaged single-level product and used to characterize the persistent wind background [12]. Accordingly, this indicator represents the persistent background wind environment at the annual scale.

Let $\overline{V}_m(s)$ be the mean 10-m wind speed in month m. The maximum monthly mean identifies the least favorable persistent-wind month while avoiding the dilution of strongly seasonal wind regimes by an annual average:

$$\begin{cases} V_y(s) = \max\limits_{1 \le m \le 12} \overline{V}_m(s), \\ \widehat{h}_{wind}(s) = \dfrac{V_y(s)}{V_y(s) + V_{75\%p}} \end{cases} \tag{23}$$

The nationwide 75th percentile is used as the characteristic transition from ordinary to significant wind conditions, compressing low-to-moderate values and improving discrimination among high-wind cells.

5.3.2 Dryness-Heavy-Rain-Induced Risk

Precipitation has a two-sided influence on land-rescue demand. Persistent precipitation deficit combined with strong atmospheric evaporative demand creates a dry background, reduces access to water in the field, increases dehydration risk, and promotes loose, dusty surface conditions. Heavy daily rainfall is abrupt and can cause waterlogging, flash floods, slope runoff, road interruption, and reduced environmental visibility. Because the two hazards operate at different temporal scales, dryness is evaluated monthly and heavy rainfall daily before they are combined into an annual index.

Daily precipitation flux and FAO-56 Penman-Monteith reference evapotranspiration for 2025 are obtained from AgERA5 v2.0.0 and used as the base variables [13, 15]. For the dry side, daily precipitation $P_d(s)$ and reference evapotranspiration $ET_{0,d}(s)$ are accumulated for month m:

$$\begin{cases} P_m(s) = \sum_{d \in m} P_d(s), \\ ET_{0,m}(s) = \sum_{d \in m} ET_{0,d}(s) \end{cases} \tag{24}$$

Following the UNEP aridity-index concept, P/PET [16], the monthly moisture supply-demand ratio is:

$$AI_m(s) = \frac{P_m(s)}{ET_{0,m}(s) + \varepsilon} \tag{25}$$

where ε is a small positive constant used to avoid division by zero. A lower $AI_m(s)$ indicates that precipitation supply is more deficient relative to atmospheric evaporative demand.
For heavy rainfall, each day is scored according to $P_d(s)$. Thresholds of 10, 25, 50, 100, and 250 mm are used to distinguish increasing precipitation intensity in accordance with the Chinese precipitation-grade standard [17]. The hazard scores assigned in this study are listed in Table 4.
Table 4 – Scoring rules for dryness and heavy-rain hazards.

Monthly moisture ratio	Dryness class	Score	Daily precipitation	Rainfall class	Score
$AI_m < 0.05$	Extreme dryness	4.00	$P_d < 10$ mm	No hazard	0.00
$0.05 \le AI_m < 0.20$	Severe dryness	2.00	$10 \le P_d < 25$ mm	Moderate rainfall	0.05
$0.20 \le AI_m < 0.50$	Significant dryness	1.00	$25 \le P_d < 50$ mm	Relatively heavy rainfall	0.25
$0.50 \le AI_m < 0.65$	Mild dryness	0.25	$50 \le P_d < 100$ mm	Heavy rain	1.00
$AI_m \ge 0.65$	No hazard	0.00	$100 \le P_d < 250$ mm	Torrential rain	2.00
-	-	-	$P_d \ge 250$ mm	Extreme torrential rain	4.00

The annual dryness and heavy-rain hazard loads are:

$$\begin{cases} D_y(s) = \frac{1}{12} \sum_{m=1}^{12} f_D[AI_m(s)], \\ R_y(s) = \min\left\{4, \frac{1}{12} \sum_{d=1}^{N_y} f_R[P_d(s)]\right\} \end{cases} \tag{26}$$

where N_y is the number of valid days in the study year, and f_D and f_R are the score mappings in Table 4. Heavy rainfall is infrequent, short-lived, and event-accumulative. Averaging directly across all days would strongly dilute its effect with a large number of non-event days. The daily scores are therefore accumulated and converted to an equivalent mean monthly load, retaining both event intensity and frequency while maintaining comparability with the monthly dryness load.
The two sides are combined with equal weights:

$$\begin{cases} Z_{DH}(s) = \eta_D D_y(s) + \eta_R R_y(s) = 0.5 D_y(s) + 0.5 R_y(s), \\ \widehat{h}_{DH}(s) = \dfrac{Z_{DH}(s)}{Z_{DH}(s) + Z_{DH,50\%p}} \end{cases} \tag{27}$$

The median annual dryness-heavy-rain load among valid land cells is used as the normalization scale, reducing the dominance of a small number of extremely dry or extremely wet cells.

5.4 Thermal-Physiological Risk Based on UTCI

The Universal Thermal Climate Index (UTCI) is used to characterize the thermal-physiological hazard of outdoor heat and cold to potentially distressed persons. UTCI is based on a human thermoregulation model and converts the combined effects of air temperature, humidity, wind speed, and

mean radiant temperature into an equivalent temperature that produces a comparable physiological response [18, 19].

Monthly UTCI statistics for 2025 are obtained from ERA5-HEAT v1.1 [14]. The official UTCI classification divides the thermal environment into ten stress categories, with 9 °C to 26 °C representing no thermal stress. The corresponding hazard scores assigned in this study are listed in Table 5.

Table 5 – UTCI stress categories and thermal-physiological hazard scores.

UTCI range	Stress category	Score
UTCI < -40 °C	Extreme cold stress	4.00
-40 °C$\leq$ UTCI < -27 °C	Very strong cold stress	2.00
-27 °C$\leq$ UTCI < -13 °C	Strong cold stress	1.00
-13 °C$\leq$ UTCI < 0 °C	Moderate cold stress	0.25
0 °C$\leq$ UTCI < 9 °C	Slight cold stress	0.10
9 °C$\leq$ UTCI $\leq$ 26 °C	No thermal stress	0.00
26 °C < UTCI$\leq$ 32 °C	Moderate heat stress	0.25
32 °C < UTCI$\leq$ 38 °C	Strong heat stress	1.00
38 °C < UTCI$\leq$ 46 °C	Very strong heat stress	2.00
UTCI > 46 °C	Extreme heat stress	4.00

Strong stress is assigned a reference score of 1, more severe stress receives progressively larger scores, the no-stress range is the zero baseline, and slight or moderate stress is assigned a lower weight.

Daily maximum and minimum UTCI represent the upper and lower bounds of the daily thermal state. Four annual components are constructed to distinguish peak and persistent hazards, as summarized in Table 6.

Table 6 – Components of the UTCI thermal-physiological hazard.

Term	UTCI statistic	Stress side	Interpretation
$HP(s)$	Daily maximum UTCI	Heat	Peak heat hazard produced by the strongest heat stress within a day
$CP(s)$	Daily minimum UTCI	Cold	Peak cold hazard produced by the strongest cold stress within a day
$HC(s)$	Daily minimum UTCI	Heat	Persistent heat hazard when even the coolest part of the day remains heat-stressed
$CC(s)$	Daily maximum UTCI	Cold	Persistent cold hazard when even the warmest part of the day remains cold-stressed

The peak components represent the mean annual loads associated with the strongest daily heat and cold stress. The persistent components represent the additional hazard caused by the absence of a daily recovery window. The annual UTCI hazard load and its normalized index are:

$$\begin{cases} UR(s) = HP(s) + CP(s) + \eta_H HC(s) + \eta_C CC(s) \\ \qquad\quad = HP(s) + CP(s) + 0.5HC(s) + 0.5CC(s), \\ \widehat{H}_{th}(s) = \dfrac{UR(s)}{UR(s) + UR_{50\%p}} \end{cases} \tag{28}$$

The nationwide median UTCI hazard load is used as the normalization scale, reducing the dominance of a small number of extremely cold or hot cells.

6. Case Study of China

The model is applied to the land area of China on the common $0.1° \times 0.1°$ grid. LDI, ANI, and ARDI are calculated to examine the framework under large-scale and geographically complex conditions. The analysis first evaluates the spatial distributions and joint behavior of LDI and ANI, identifying concentrations of potential land-rescue demand and areas where ground response is constrained. It then examines the spatial and cumulative distributions of ARDI. Finally, representative critical scenarios with clear physical interpretations are used to partition the continuous indices into five

functional zones: low demand, ground-dominant, aviation-assisted, aviation-dependent, and high-aviation-demand.

6.1 ANI and LDI Distribution

LDI and ANI both exhibit strong spatial heterogeneity, but their dominant gradients run in opposite directions, as shown in Figure 1. LDI is generally higher in eastern and southern China and lower in the western interior. ANI is higher across western plateaus and border regions and lower in eastern plains and urbanized areas. High-value coupling mainly occurs in transition zones where mountains, plateaus, or deserts intersect with areas of sustained human activity.

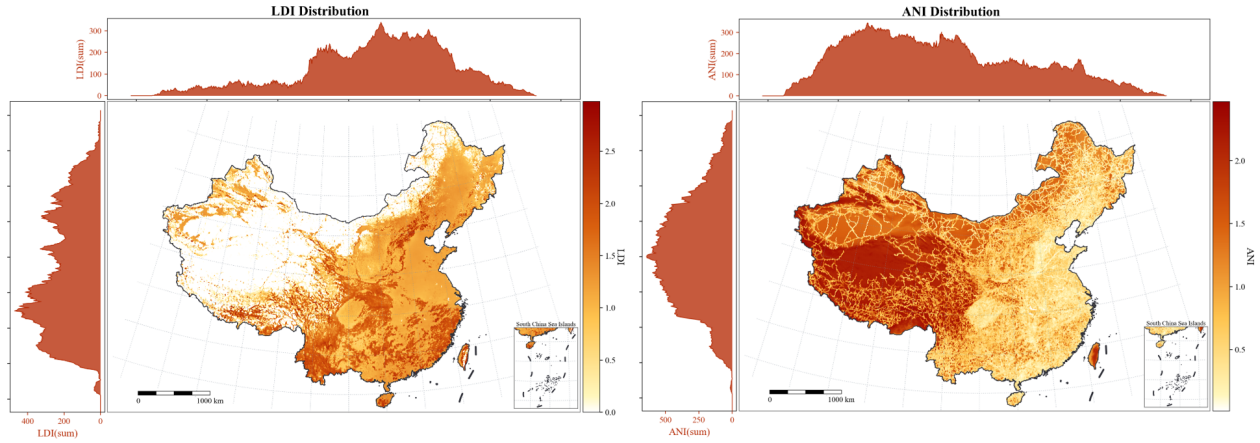


Figure 1 – Geographic distributions of LDI and ANI in China.

6.1.1 Spatial Distribution of LDI

At the national scale, LDI is more spatially continuous in the east and more fragmented in the west, with higher levels in central-eastern and southern China and lower levels in the western interior. Continuous or semi-continuous high-value areas occur around the Sichuan Basin, on the Yunnan-Guizhou Plateau, in parts of the middle and lower Yangtze region, and across the southeastern hills. These areas combine relatively high population exposure with one or more environmental hazards. The North China Plain, Northeast China Plain, and Loess Plateau contain continuous population distributions but generally moderate environmental hazards; they therefore show predominantly medium LDI, with local peaks near mountain-plain interfaces and population centers.

In western China, LDI follows oases, river valleys, piedmont zones, and transport corridors. Narrow or discontinuous demand belts are visible along the northern and southern flanks of the Tianshan Mountains, the margin of the Tarim Basin, the Hexi Corridor, the margin of the Qaidam Basin, and the Yarlung Zangbo valley. Despite harsh natural conditions, the Taklamakan Desert, the interior of the Tibetan Plateau, the Gobi, and other areas with extremely low human activity retain LDI values close to zero. This spatial pattern reflects the intended coupling of population exposure and environmental hazards in the LDI formulation.

6.1.2 Spatial Distribution of ANI

ANI displays a clearer west-high/east-low and mountain-high/plain-low pattern. Most of Tibet, southern and western Qinghai, the western Sichuan Plateau, and parts of the high mountains and deserts of Xinjiang form continuous or extensive high-value areas because roads are sparse and terrain constraints are strong. Other parts of Xinjiang, western Gansu, eastern Qinghai, western Inner Mongolia, the Hengduan Mountains, and forested border mountains in Northeast China form transition belts from high to moderate aerial necessity.

The Yunnan-Guizhou Plateau, Qinling Mountains, southeastern hills, and other mountain-plain transition zones generally show moderate ANI. Ground-response infrastructure exists, but access can still be affected by relief, circuitous roads, and localized bottlenecks. In contrast, the Northeast China Plain, North China Plain, middle and lower Yangtze Plain, Pearl River Delta, and Sichuan Basin have

dense road networks and limited terrain constraints. ANI is consequently low, and aviation is more likely to provide rapid reinforcement or specialized support than to serve as the primary means of routine access.

6.1.3 Joint Distribution of ANI and LDI

Joint sampling of valid land cells reveals pronounced clustering, elongation, and stratification in the ANI-LDI space (Figure 2). Most cells concentrate in the low-ANI, medium-to-high-LDI region, whereas high-ANI cells form vertical distributions extending from near-zero to medium or high LDI.

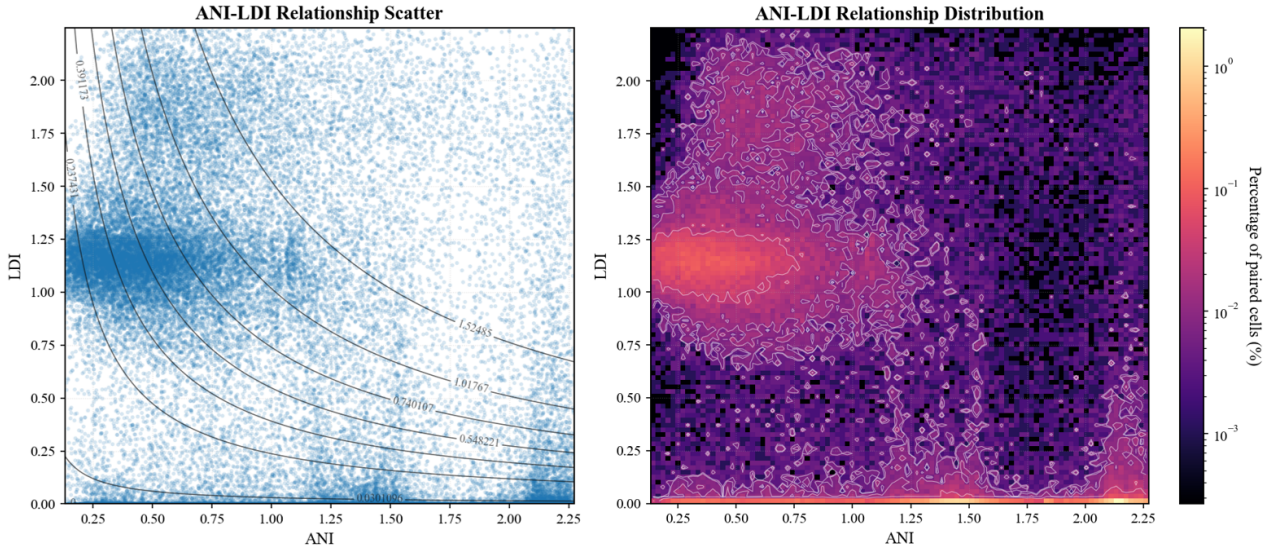


Figure 2 – Joint distribution of ANI and LDI for valid land cells in China.

The principal low-ANI, medium-to-high-LDI cluster corresponds to central and eastern plains, urban agglomerations, and basins, where human activity and potential demand are substantial but ground response can readily substitute for aerial response. The low-to-moderate-ANI, high-LDI region corresponds mainly to the Yunnan-Guizhou Plateau, southeastern hills, the margins of the Sichuan Basin, and other mountain-plain interfaces. Here, relatively high demand coexists with moderate access constraints, favoring an air-ground collaborative mode.

Several vertical bands at ANI values of approximately 1.25–1.50 correspond primarily to Xinjiang, Qinghai, western Gansu, and western Inner Mongolia. They reflect rapid transitions between sparsely populated desert or high-mountain cells and nearby oases, valleys, and towns. High-ANI, low-LDI cells occur mainly in the Tibetan interior, western Qinghai, and high-mountain or desert areas of Xinjiang. Individual missions in these cells may depend strongly on aviation, but aggregate rescue demand remains limited. Medium-to-high-ANI, medium-to-high-LDI cells occur mainly in the southern Tibetan valleys, the Hengduan Mountains, populated belts of western Sichuan, the flanks of the Tianshan Mountains, and selected western mountain towns. These areas form the primary spatial basis of high ARDI.

6.2 ARDI Distribution

6.2.1 Spatial Distribution of ARDI

Coupling LDI and ANI yields the national ARDI distribution shown in Figure 3. High values are not spatially continuous; instead, they concentrate in mountain, plateau, and border-transition zones where population activity, environmental hazards, and ground-access constraints overlap. The spatial pattern can be descriptively summarized as four principal regions, four secondary belts, and one island.

The four principal regions are Southern Tibet, the Hengduan Mountains, the Qinghai-Gansu mountain region, and Xinjiang. High values in Southern Tibet follow the Yarlung Zangbo valley, border mountains, and population nodes. In the Hengduan Mountains, populated corridors intersect with highly dissected terrain, forming the most continuous high-value core. The Qinghai-Gansu region

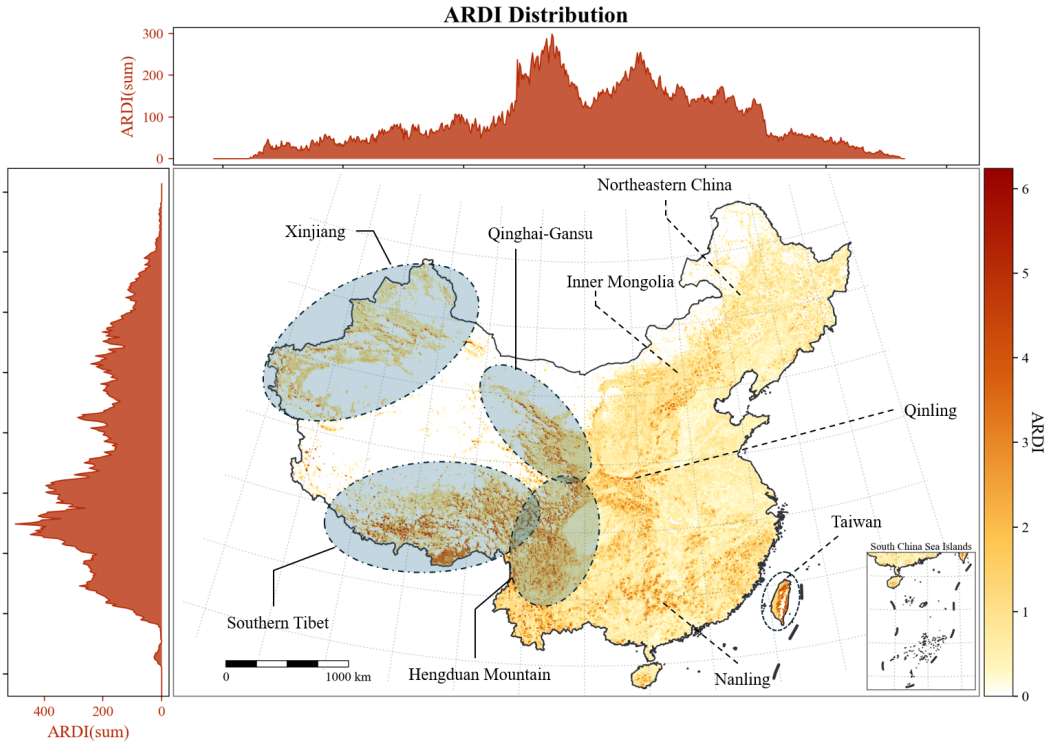


Figure 3 – Geographic distribution of ARDI in China.

reflects the combined influence of plateau mountains, transport corridors, and dispersed settlements. In Xinjiang, high values follow the northern and southern Tianshan piedmonts, oasis margins, mountain fronts, and urban nodes. These regions are not uniformly high-demand: deserts and uninhabited plateau interiors remain low because of insufficient population exposure.

The four secondary belts are the Greater Khingan Range, the Qinling Mountains, northern Inner Mongolia, and the Nanling Mountains. They are smaller than the four principal regions but follow distinct mountain- or border-oriented patterns. The Greater Khingan and northern Inner Mongolia belts are influenced by weak road support, large spatial extent, and dispersed population. The Qinling and Nanling belts lie between relatively populated regions, where local high demand is generated by mountain barriers, environmental hazards, and surrounding human activity.

The island is Taiwan Island, where high values are concentrated in the Central Mountain Range and its transition toward the populated coastal zone.

6.2.2 Cumulative Distribution of ARDI

A critical ARDI value, $ARDI_{cr}$, is derived from a representative compound scenario with a clear planning interpretation. The scenario assumes: ambient population at or above the 25th percentile among populated cells; at least two of the three hazard dimensions at their half-response levels; road density at or below the 25th percentile among road-covered cells; and the full RDLS index at or above the national 75th percentile. Substituting these half-response conditions into the model gives:

$ARDI_{cr} = 0.78125.$

This scenario represents a cell with sustained ambient-population exposure, at least two representative environmental hazards, and clear constraints on ground rescue from both road support and terrain. The relative necessity of aerial intervention therefore reaches a planning-significant level. The cumulative ARDI distribution, marked by this threshold, is shown in Figure 4. The threshold is exceeded by 28.61% of the valid area.

The distribution is strongly nonlinear and long-tailed. Roughly the lowest 30% of cells lie near the horizontal axis and have ARDI values close to zero. They include areas with extremely low population activity and areas where population is present but environmental hazards or aerial necessity remain low. Cells between approximately the 30th and 78th percentiles form a slowly rising interval representing most of China's land area with low-to-moderate aerial-rescue demand; aerial intervention

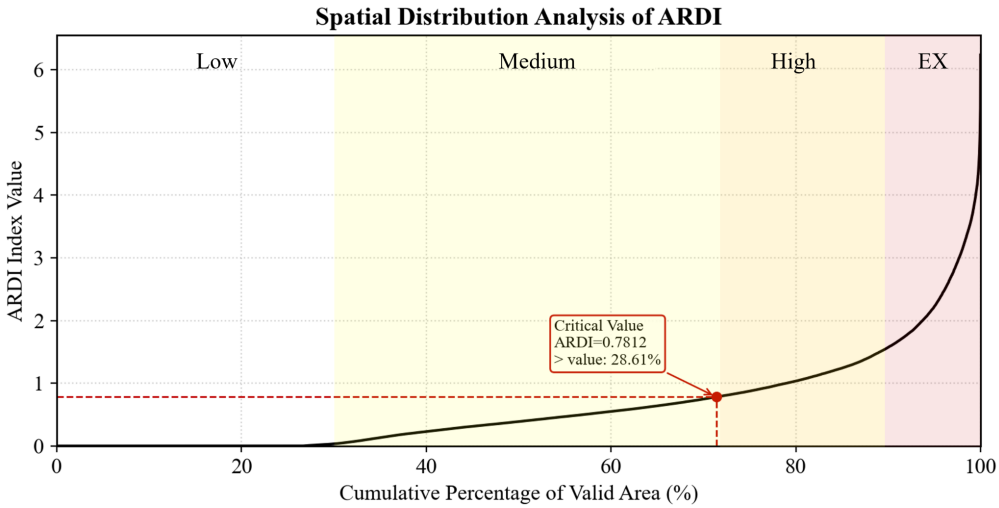


Figure 4 – Cumulative distribution of ARDI over valid land cells in China.

retains a supplementary role.

From the vicinity of the critical threshold to about the 90th percentile, the slope increases markedly, indicating stronger coupling among population activity, environmental hazards, and ground-access constraints. These cells correspond mainly to the margins of core high-value regions, secondary demand belts, and populated mountain nodes. Roughly the upper 10% form the steep long tail, representing extreme combinations of high land-rescue demand and high aerial necessity. These cells define the highest-priority portion of the national aerial-rescue demand basemap.

6.3 Air-Ground Operational Boundary Zones

Four thresholds are established from representative combinations of ambient-population exposure, environmental hazards, road support, and terrain constraints: the minimum effective land-rescue-demand threshold τ_{L0}, the high land-rescue-demand threshold τ_{L1}, the aerial-relative-necessity threshold τ_N, and the significant aerial-demand threshold τ_A. Their values and interpretations are given in Table 7.

Table 7 – Thresholds for demand-side air-ground functional zoning.

Threshold	Value	Representative critical condition	Decision function
τ_{L0}	0.25000	$P_a \geq P_{a,25\%nzp}$; at least one environmental hazard at half response	Separates low-demand cells from cells with effective land-rescue demand
τ_{L1}	1.18750	$P_a \geq P_{a,25\%nzp}$; all three environmental hazards at half response	Identifies high compound land-rescue demand
τ_N	1.25000	$RD \leq RD_{25\%nzp}$ and $RDLS \geq RDLS_{75\%p}$	Separates ground-dominant and aviation-dependent demand conditions
τ_A	0.78125	$P_a \geq P_{a,25\%nzp}$; at least two hazards at half response; $ANI \geq \tau_N$	Identifies planning-relevant aerial-rescue demand

For terrain-induced risk, half response corresponds to local relative relief at the nationwide 75th percentile. For weather-induced risk, the representative condition places both wind and dryness-heavy-rain hazards at their respective characteristic scales. For thermal-physiological risk, half response corresponds to an annual UTCI hazard load at the nationwide median. For ANI, the half-response levels correspond to road density at the lower quartile of road-covered cells and the full RDLS index at the nationwide upper quartile.

The minimum effective demand threshold, $\tau_{L0} = 0.25$, represents sustained ambient-population exposure combined with at least one representative environmental hazard and marks the point at which potential demand becomes non-negligible. The high-demand threshold, $\tau_{L1} = 1.1875$, corresponds to all three hazard dimensions at half response and represents a fully developed compound environmental effect. The aerial-necessity threshold, $\tau_N = 1.25$, represents simultaneous half responses for road-

support deficiency and terrain constraint and marks the principal transition from ground-dominant to aviation-dependent response. The significant aerial-demand threshold, $\tau_A = 0.78125$, combines sustained ambient-population exposure, two hazards at half response, and significant ground constraints.

Applying these thresholds partitions China's land area into the five functional zones shown in Figure 5.

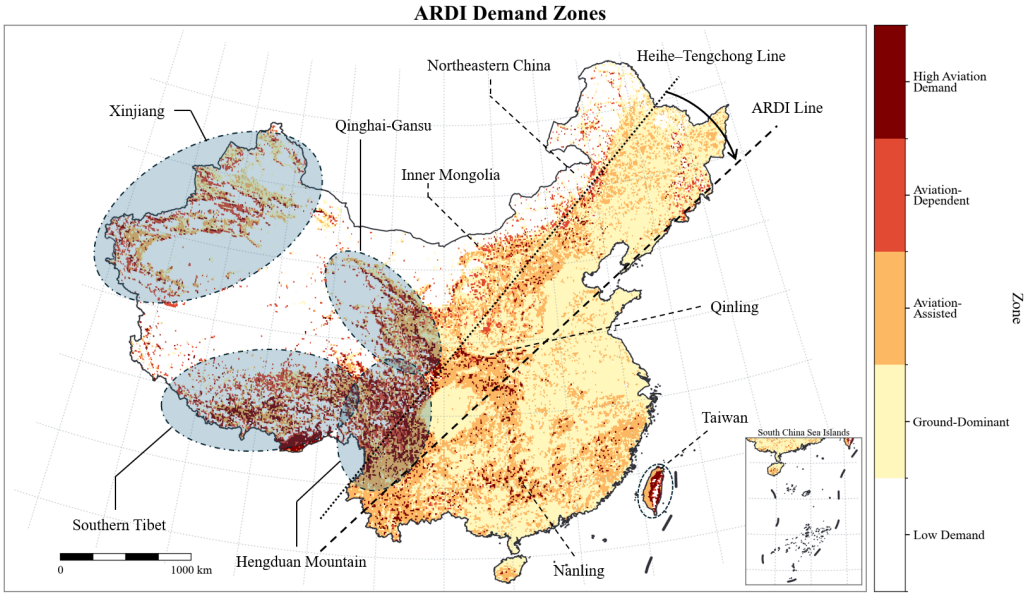


Figure 5 – Geographic distribution of demand-side air-ground functional zones in China.

Low-demand zones are concentrated in western plateaus, deserts, and other areas with sparse human activity, as well as in some plain cells with low environmental hazards. Ground-dominant zones are widespread across central and eastern plains, basins, and well-connected areas. Rescue demand is non-negligible, but ground response can readily substitute for aerial response. Aviation-assisted zones occur mainly in densely populated hills, mountain margins, and areas with comparatively weak transport access. Ground-access conditions remain comparatively favorable, while the local demand level gives aerial intervention clear relative value.

Aviation-dependent zones occur around western oasis and valley margins, border mountains, and parts of the plateau with dispersed populations. Demand remains below the high-demand threshold, while strong ground-mobility constraints produce a high relative necessity for aerial response. High-aviation-demand zones concentrate in Southern Tibet, the Hengduan Mountains, the Qinghai-Gansu mountain region, the mountains of Xinjiang, and selected secondary mountain belts. Both rescue demand and aerial necessity are high, making these areas the highest-priority components of the national aerial-rescue demand basemap.

At the national scale, the functional zoning shows a pronounced east-west contrast and suggests an approximate northeast-southwest ARDI line. Excluding the extensive uninhabited areas of western China, locations west of this line generally exhibit greater dependence on aerial response and higher aerial-rescue demand, whereas locations east of it are more often ground-dominant or aviation-assisted.

The overall orientation of the ARDI line resembles the Heihe-Tengchong Line, but the two have different mechanisms and do not coincide spatially. They are relatively close in the southwest because population activity, relief, and road coverage all exhibit strong gradients across the Tibetan Plateau-Hengduan Mountains-Sichuan Basin transition, producing similar gradients in population distribution and aerial-rescue demand. Toward the northeast, the two lines diverge and the ARDI line shifts eastward. Although the Greater Khingan Range and northeastern border forests are less populated than the central and eastern plains, weak road support and stronger terrain constraints maintain relatively high ANI.

Conversely, across most plains, basins, and urbanized areas east of the Heihe-Tengchong Line, high ambient-population exposure is offset by dense road networks that substantially increase the extent to which ground response can substitute for aerial response. Most of these areas are therefore ground-dominant or aviation-assisted.
The mathematical criteria and area shares of the five zones are summarized in Table 8.
Table 8 – Demand-side air-ground functional-zone classification and area shares for China.

Zone	Mathematical criterion	Share of valid land cells
Low demand	$L(s) < 0.25000$	37.62%
Ground-dominant	$L(s) \geq 0.25000$, $N(s) < 1.25000$, $A(s) < 0.78125$	32.06%
Aviation-assisted	$L(s) \geq 0.25000$, $N(s) < 1.25000$, $A(s) \geq 0.78125$	19.23%
Aviation-dependent	$0.25000 \leq L(s) < 1.18750$, $N(s) \geq 1.25000$	5.92%
High-aviation-demand	$L(s) \geq 1.18750$, $N(s) \geq 1.25000$	5.16%

Low-demand and ground-dominant zones account for 37.62% and 32.06% of valid cells, respectively, indicating that most land cells either lack significant rescue demand or exhibit demand-access conditions associated with ground-dominant response. Aviation-assisted zones account for 19.23% and form the main spatial range in which aerial response has increased relative value. Aviation-dependent and high-aviation-demand zones account for 5.92% and 5.16%, respectively. The former is characterized by a high relative necessity for aerial response under low-to-moderate demand, while the latter represents priority areas where demand and aerial necessity are both high.
Together, the aviation-assisted, aviation-dependent, and high-aviation-demand zones account for 30.31% of valid land cells, indicating that approximately three-tenths of the effective land grid has some degree of planning value for aerial intervention. The aviation-dependent and high-aviation-demand zones together account for 11.08%, indicating strong dependence on aerial response across approximately one-tenth of the valid land area.

7. Conclusions

This study developed the Aerial Rescue Demand Intensity index and a corresponding spatial-analysis method to address the lack of a quantitative demand surface and a unified demand-side air-ground boundary for large-scale land SAR. The framework was applied to China to calculate demand intensity, identify spatial patterns, and establish demand-side air-ground functional zones. The principal findings are as follows.

(1) ARDI is constructed from Land Rescue Demand Intensity and the Aerial Relative Necessity Index. LDI uses ambient population as a proxy for the size of the potentially exposed population and incorporates terrain-induced, weather-related, and thermal-physiological hazards. ANI uses road-support deficiency and terrain constraints to characterize the extent to which ground-access conditions allow ground response to substitute for aerial response. Their multiplicative coupling identifies areas that simultaneously contain meaningful rescue demand and a high relative necessity for aerial response. This structure assigns high ARDI only to cells where meaningful demand and aerial necessity coexist. The component modules can be replaced or extended for different data environments and mission contexts.

(2) LDI and ANI exhibit opposing but coupled spatial gradients. LDI is generally higher in eastern and southern China and lower in the western interior, while ANI is higher across western plateaus and border regions and lower in eastern plains and urbanized areas. Their coupling produces ARDI hotspots primarily where human activity intersects complex mountains, plateaus, and border-transition environments. The resulting pattern can be descriptively summarized as four principal regions - Southern Tibet, the Hengduan Mountains, the Qinghai-Gansu mountain region, and Xinjiang - four secondary belts - the Greater Khingan Range, the Qinling Mountains, northern Inner Mongolia, and the Nanling Mountains - and one island, Taiwan Island.

(3) A demand-side functional zoning method was established using thresholds for minimum effective land demand, high land demand, aerial relative necessity, and significant aerial demand. China's land cells were classified into low-demand, ground-dominant, aviation-assisted, aviation-dependent, and high-aviation-demand zones, accounting for 37.62%, 32.06%, 19.23%, 5.92%, and 5.16% of valid cells, respectively. The three zones with clear value for aerial intervention account for 30.31%, while the aviation-dependent and high-aviation-demand zones together account for 11.08%.

Overall, the study provides an integrated demand-side method linking demand identification, aerial-necessity assessment, composite intensity calculation, and air-ground functional zoning. The resulting demand basemap quantitatively represents the spatial intensity and distribution of aerial-rescue demand and supports regional demand prioritization.

8. Contact Author Email Address

Contact author: makarovwang@163.com

9. Copyright Statement

The authors confirm that they, and/or their company or organization, hold copyright on all of the original material included in this paper. The authors also confirm that they have obtained permission, from the copyright holder of any third-party material included in this paper, to publish it as part of their paper. The authors confirm that they give permission, or have obtained permission from the copyright holder of this paper, for its publication and distribution as part of the ICAS proceedings or as individual off-prints from the proceedings.

References

[1] Stone K L, Smedley W A, Killian J T, et al. Aeromedical retrieval of trauma patients: Impact of flight path model on estimates of population coverage. *The American Journal of Surgery*, Vol. 220, No. 3, pp 765–772, 2020. DOI: 10.1016/j.amjsurg.2020.01.056.

[2] Razi N, Karatas M and Gunal M M. A combined optimization and simulation-based methodology for locating search and rescue helicopters. *Proceedings of the 49th Annual Simulation Symposium (ANSS 2016)*, Pasadena, CA, pp 31–38, 2016. DOI: 10.22360/SpringSim.2016.ANSS.009.

[3] Zhang F, Peng X, Sun Y F, Yu Q and Wen Y. An optimized site selection method for human-life search and rescue in inland waters. *ASCE-ASME Journal of Risk and Uncertainty in Engineering Systems, Part A: Civil Engineering*, Vol. 10, No. 3, 04024036, 2024. DOI: 10.1061/AJRUA6.RUENG-1166.

[4] Keeney R L and Raiffa H. *Decisions with multiple objectives: Preferences and value trade-offs*. Cambridge University Press, Cambridge, 1993. DOI: 10.1017/CBO9781139174084.

[5] OECD, European Union and European Commission Joint Research Centre. *Handbook on constructing composite indicators: Methodology and user guide*. OECD Publishing, Paris, 2008. DOI: 10.1787/9789264043466-en.

[6] De Groeve T, Poljansek K and Vernaccini L. *Index for Risk Management – INFORM: Concept and methodology*. Publications Office of the European Union, Luxembourg, 2014. DOI: 10.2788/78658.

[7] Haklay M and Weber P. OpenStreetMap: User-generated street maps. *IEEE Pervasive Computing*, Vol. 7, No. 4, pp 12–18, 2008. DOI: 10.1109/MPRV.2008.80.

[8] Feng Z M, Tang Y, Yang Y Z and Zhang D. The relief degree of land surface in China and its correlation with population distribution. *Acta Geographica Sinica*, Vol. 62, No. 10, pp 1073–1082, 2007. DOI: 10.11821/xb200710007.

[9] You Z, Feng Z M and Yang Y Z. Relief degree of land surface dataset of China (1 km). *Digital Journal of Global Change Data Repository*, 2018. DOI: 10.3974/geodb.2018.03.16.V1.

[10] Lebakula V, Gonzales J, Stipek C, et al. *LandScan Global 2024*. Dataset, Oak Ridge National Laboratory, Oak Ridge, TN, 2025. DOI: 10.48690/1532445.

[11] Dobson J E, Bright E A, Coleman P R, Durfee R C and Worley B A. LandScan: A global population database for estimating populations at risk. *Photogrammetric Engineering & Remote Sensing*, Vol. 66, No. 7, pp 849–857, 2000.

[12] Copernicus Climate Change Service. ERA5 monthly averaged data on single levels from 1940 to present. *Climate Data Store*, 2019. DOI: 10.24381/cds.f17050d7.

[13] Copernicus Climate Change Service. Agrometeorological indicators from 1979 to present derived from reanalysis. *Climate Data Store*, 2020. DOI: 10.24381/cds.6c68c9bb.

[14] Copernicus Climate Change Service. Thermal comfort indices derived from ERA5 reanalysis. *Climate Data Store*, 2020. DOI: 10.24381/cds.553b7518.

[15] Allen R G, Pereira L S, Raes D and Smith M. *Crop evapotranspiration: Guidelines for computing crop water requirements*. FAO Irrigation and Drainage Paper No. 56, Food and Agriculture Organization of the United Nations, Rome, 1998.

[16] Middleton N and Thomas D. *World atlas of desertification*. United Nations Environment Programme and Edward Arnold, London, 1992.

[17] General Administration of Quality Supervision, Inspection and Quarantine of the People's Republic of China and Standardization Administration of China. *Grade of precipitation: GB/T 28592-2012*. Standards Press of China, Beijing, 2012.
[18] Brode P, Fiala D, Blazejczyk K, Holmér I, Jendritzky G, Kampmann B, Tinz B and Havenith G. Deriving the operational procedure for the Universal Thermal Climate Index (UTCI). *International Journal of Biometeorology*, Vol. 56, No. 3, pp 481–494, 2012. DOI: 10.1007/s00484-011-0454-1.
[19] Blazejczyk K, Jendritzky G, Brode P, Fiala D, Havenith G, Epstein Y, Psikuta A and Kampmann B. An introduction to the Universal Thermal Climate Index (UTCI). *Geographia Polonica*, Vol. 86, No. 1, pp 5–10, 2013. DOI: 10.7163/GPol.2013.1.